The effect of layer thickness on the optical parameters of phase-change material Sb_2Te_3

© A.A. Gavrikov[1], V.G. Kuznetsov[2], N.E. Dyadkina[1], A.V. Kolobov[1]

[1] Institue of Physics and Research and Development Institute of Physical Research,
Herzen Russian State University,
191186 St. Petersburg, Russia
[2] Ioffe Institute,
St. Petersburg, Russia

E-mail: agavrikov@herzen.spb.ru

Received November 12, 2025
Revised December 2, 2025
Accepted January 9, 2026

Antimony telluride (Sb_2Te_3) is one of the promising phase-change materials used in memory and data processing devices. Its layered structure allows for the fabrication of extremely thin layers with a thickness of about 1 nm. However, the issue of maintaining the contrast of properties between the amorphous and crystalline phases in extremely thin layers of Sb_2Te_3 has not yet been studied. In this study, the density functional theory calculations were used to perform a comparative analysis of the amorphous phase structure and optical property contrast for layers with a thickness of 1 ML, 2 ML and the bulk material. It was demonstrated that the optical property contrast is preserved down to 1 monolayer.

Keywords: phase-change materials, Sb_2Te_3, monolayer, optical contrast, DFT method

DOI: 10.61011/SC.2026.01.63724.8774

1. Introduction

Phase-change materials are commonly referred to as materials that can reversibly transit from an amorphous state to a crystalline one and at the same time have a significant contrast in properties between these two phases [1–3]. Most of such materials are the chalcogenides of antimony and tellurium. Due to these properties, the phase-change materials have found wide application in optical memory devices (rewritable optical discs from CD to Blu-ray) [4] and in non-volatile electronic memory, the latest implementation of which was Optane(R) memory, released in 2015 by Intel and Micron [5,6]. Recently, the phase-change chalcogenides have also been considered as leading candidates for the development of electronic and photonic neuromorphic networks [7–9].

Traditionally, the phase-change memory devices use compositions along a quasi-binary section of GeTe-Sb_2Te_3, e. g., $Ge_2Sb_2Te_5$ [10,11]. However, recently, an ever-growing attention has been paid to the two-dimensional chalcogenides, in particular transition metal dichalcogenides, where a rapid photoinduced transition between semiconductor and metallic states is observed [12–14]. At the same time, it was shown that Sb_2Te_3, which is a layered van der Waals crystal and one of the extreme points of a quasi-binary section, is itself an phase-change material [15,16]. The structure of Sb_2Te_3 is illustrated in Figure 1, *a*. The material is a layered or two-dimensional structure in the sense that it consists of covalently bonded layers connected by a way weaker Van der Waals forces. In English-language literature, such layers are commonly referred to as quintuple layers. In terms of the layered structure of a two-dimensional material, this layer is also often referred to as a monolayer (ML). We'll use this terminology here.

It is interesting to note that Sb_2Te_3 is a classical topological insulator [17]. In this class of materials, the surface plays a specific role. Unlike conventional insulators or semiconductors, in which surface states are usually localized, topological insulators have protected surface states that arise due to the topological properties of the bulk

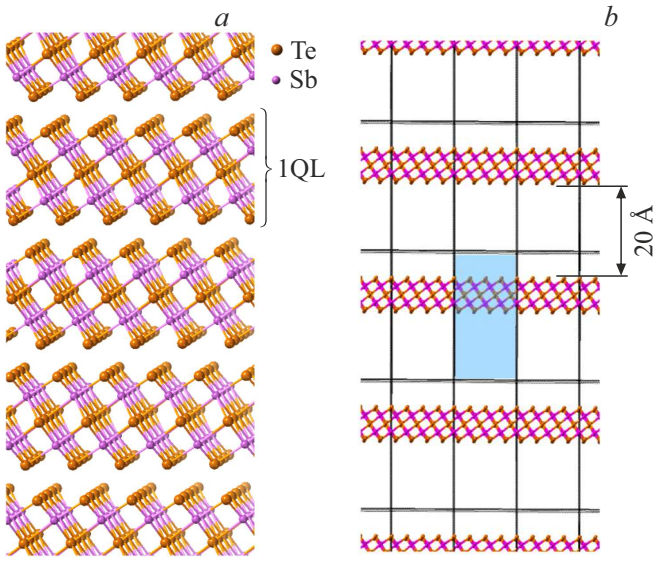

Figure 1. The structure of the bulk crystal Sb_2Te_3 (*a*) and ultathin layers of 1QL in the model of a periodic plate (*b*).

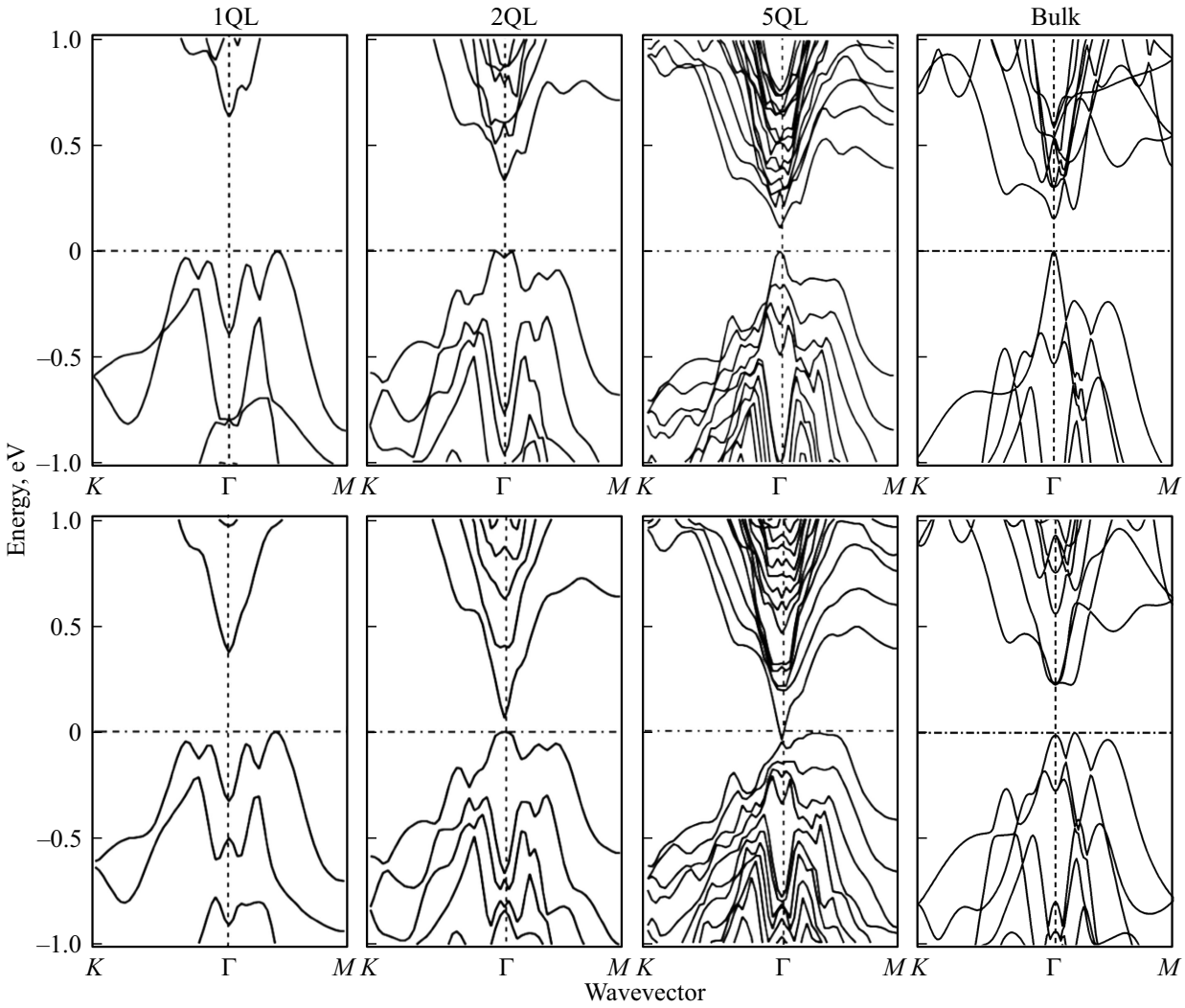

Figure 2. Band diagrams for ultrathin layers and bulk Sb_2Te_3, calculated both without and with spin-orbital interaction.

band structure. On the surface of a topological insulator, electrons with opposite spins move in opposite directions, which is associated with a strong spin-orbit interaction and ensures stability of such states to non-magnetic impurities. The surface states are characterized by linear dispersion, the so-called Dirac cone. At that, these states may occur only with the layer thickness Sb_2Te_3 being larger than 5–6 monolayers.

Figure 2 shows the band diagrams for ultrathin layers and bulk Sb_2Te_3, calculated by the authors using the density functional theory (DFT) method in the spin-unpolarized version (Sb_2Te_3 is a non-magnetic material) both, accounting for the spin-orbit interaction and neglecting it. It can be seen that the band gap decreases monotonously as the layer becomes thicker, and with thicknesses of 5–6 monolayers, the material becomes a topological insulator (a Dirac cone is formed). This result indicates a pronounced dependence of the properties of layered Sb_2Te_3 on its thickness. In bulk materials, the energy gap is not closed.

Another vivid illustration of the electronic structure (and its properties) dependence on thickness are the layered transition metal dichalcogenides, an example of which is MoS_2. As indirect band gap semiconductors in case of a bulk material, they become direct band gap in the limit of one monolayer [18].

It is also known that the stability of the amorphous phase may depend on the layer thickness [19], which brings us directly to the task of this study — to determine the effect of the thickness of Sb_2Te_3 layer on its phase-change properties.

2. Calculation method

The calculations were made using the density functional method in the spin-unpolarized version within the generalized gradient approximation (GGA) with an exchange-correlation functional in the form of PBE [20], implemented in the plane-wave pseudopotential code CASTEP (Cambridge Serial Total Energy Package) [21,22]. Van der

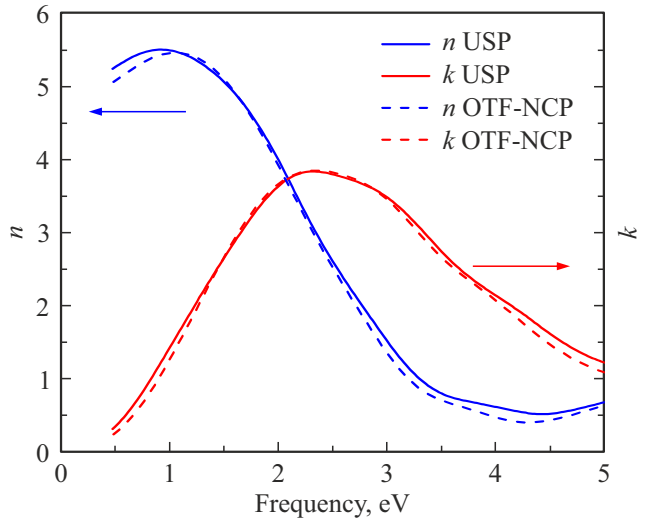

Figure 3. Optical constants calculated with USP pseudopotentials and OTF-NCP.

Waals (VdW) interaction was taken into account using the VdW correction Grimme D2 [23], and the electron-ion interaction — using Vanderbilt ultra-soft pseudopotentials (USP) [24].

Amorphous bulk phase Sb_2Te_3 (a-Sb_2Te_3) was obtained *in silico* by *ab initio* molecular dynamics method (AIMD) by melting the crystalline phase as per standard protocol [25,26]: a) to account for the material thermal expansion with further use of NVT ensemble the linear dimensions of a hexagonal unit cell (UC)) of Sb_2Te_3 crystal were enlarged by 2 %, after which using the same UC a supercell was constructed with an expansion $4\times4\times1$, containing 240 atoms; b) next, to destruct the far-range order peculiar to the crystal the obtained structure was melted and randomized with the help of NVT ensemble and Langevin thermostat at $T = 3000$ K for 20 ps with a step of 2 fs; c) the randomized structure was then cooled down to $T = 1000$ K (slightly higher than the melting temperature of $T_m = 900$ K) with a rate of 100 K/ps and equilibrated at this temperature with a step of 2 fs during 20 ps; d) after this, the obtained structure was quenched with a cooling rate of 100 K/ps to a room temperature of $T = 300$ K during 14 ps with a step of 2 fs.

Amorphous layers consisting of one (1QL) and two (2QL) fivefold monolayers were considered in the supercell approximation in the periodic slab model with the number of atoms 80 and 160, respectively, in a supercell with the $4\times4\times1$ extension and were also generated *in silico* by AIMD method using a protocol similar to the one described above, with the only difference that at the melting stage of 1QL and 2QL fivefold monolayers at a temperature of $T = 3000$ K, in order to prevent „evaporation“ of the material, the vacuum in supercell $4\times4\times1$, used for analysis in the periodic slab model, was uniformly filled with atoms of an inert gas (argon).

Calculations of the optical constants of all the crystalline and amorphous structures studied in the work were performed with USP pseudopotentials. To verify the results, one analysis was also performed with on-the-fly norm-conserving (more „expensive“ in terms of computational resources) pseudopotentials OTF-NCP [21,22], and from Figure 3 it is clear that the results differ only slightly.

Within the framework of DFT method, optical spectra resulting from single-particle electronic transitions between occupied and unoccupied Kohn-Sham states can be considered [27] as a joint density of states between the valence band and the conduction band, weighted with the probability of interband optical transitions, taking into account the selection rules. CASTEP first calculates $\varepsilon_2(\omega) = Im\big(\varepsilon(\omega)\big)$ (imaginary part of the dielectric permittivity) using the expression similar to the golden rule of Fermi for the time-dependent pertubations [21,22]:

$$\varepsilon_2(\omega) = \frac{2e^2\pi}{\epsilon_0\Omega}\sum_{k,v,c}|\langle\psi_k^c|\mathbf{u}\cdot\mathbf{r}|\psi_k^v\rangle|^2\delta(E_k^c - E_k^v - \hbar\omega), \quad (1)$$

where $\mathbf{u}$ is the unit polarization vector of the electric field of the incident photon, $\mathbf{r}$ is the coordinate operator, e is the electron charge, Ω is the volume of the unit cell, ε_0 is the dielectric constant of the vacuum. The wave functions ψ_k^c and ψ_k^v describe the states of the conduction band and the valence band with eigen values E_k^c and E_k^v, respectively, obtained as self-consistent solutions of the Kohn-Sham equations [21,22] in a pseudopotential formalism for optimized structure geometry. The Brillouin zone (BZ) integration was performed on a discrete set of k-points of the Monkhorst-Pack [28] grid, the partition of which for all calculated structures was chosen so that the distance between neighboring k-points of the BZ (actual k-spacing) was equal to $\sim 0.03\,\text{A}^{-1}$, which ensured consistent calculation precision for different structures. The cutoff E_{cutoff} of kinetic energy were taken to be 300 eV for USP pseudopotentials and 700 eV for OTF-NCP pseudopotentials.

It should be stressed that when calculating $\varepsilon_2(\omega)$ using the formula (1) the following approximations were used: a) the electric dipole approximation for matrix elements of optical transitions; b) the effects of the local field (the effect of the polarizability of the crystal on the electric field inside the material) are not taken into account; c) exciton effects are not taken into account; d) an approximation related to the use of pseudo-wave functions in the calculation of matrix elements of optical transitions instead of full-electron wave functions [21,22].

The real and imaginary parts of the dielectric function $\varepsilon(\omega)$ are related by Kramers–Kronig transform [29]:

$$Re\big(\varepsilon(\omega)\big) = 1 + \frac{2}{\pi}\int_0^\infty \frac{Im\big(\varepsilon(\omega')\big)\omega' d\omega'}{\omega'^2 - \omega^2}, \quad (2)$$

which further helps to calculate $\varepsilon_1(\omega) = Re\big(\varepsilon(\omega)\big)$ (real part of the dielectric function). And finally, CASTEP

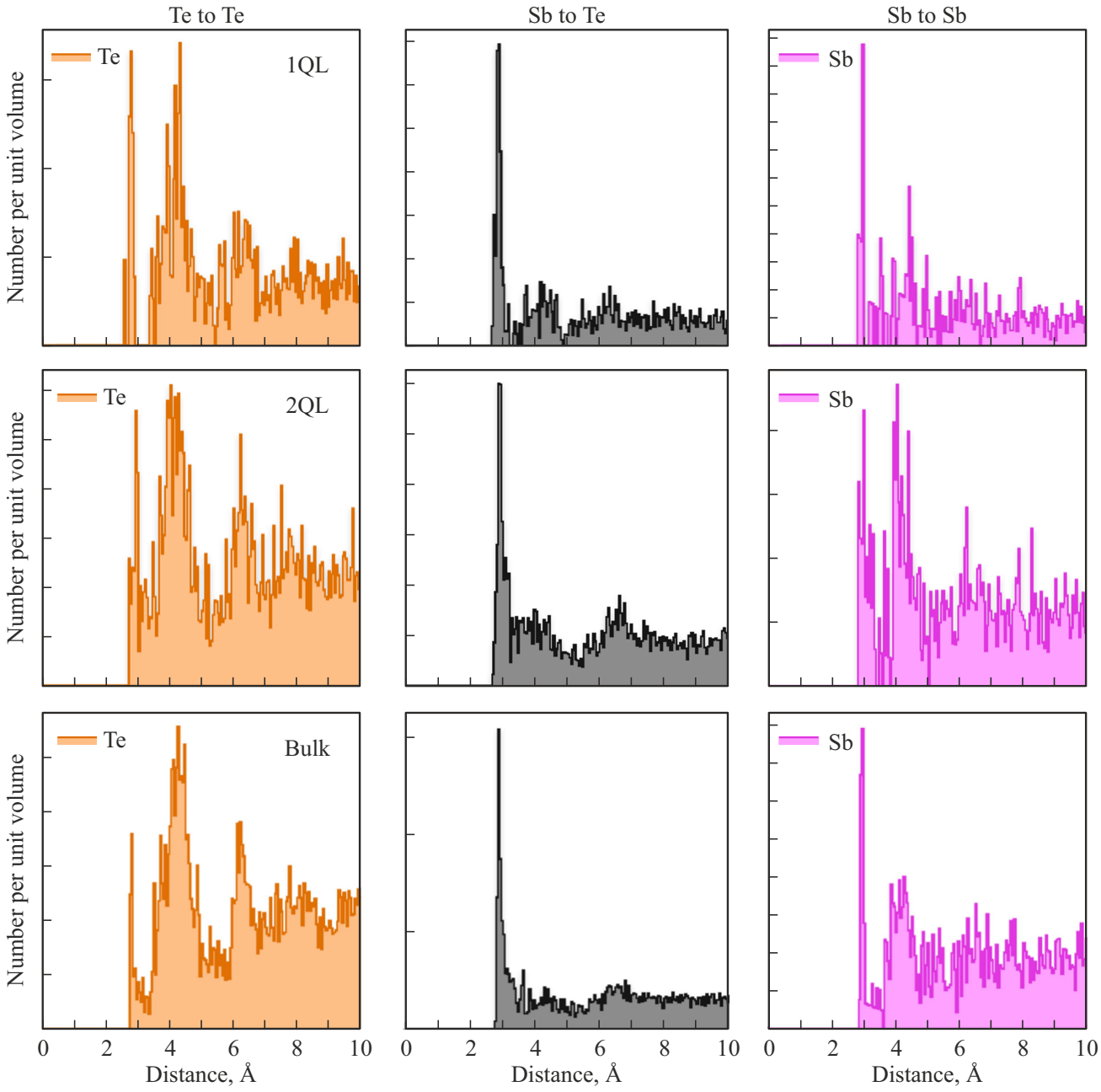

Figure 4. Correlation functions for central Sb and Te atoms in the amorphous phase for ultrathin layers and bulk material.

calculates the spectral dependencies of the refractive indices n and extinction coefficients k using simple formulae expressing n and k via $\varepsilon_1(\omega)$ and $\varepsilon_2(\omega)$:

$$n = \sqrt{\frac{\sqrt{\varepsilon_1^2 + \varepsilon_2^2} + \varepsilon_1}{2}}, \quad (3)$$

$$k = \sqrt{\frac{\sqrt{\varepsilon_1^2 + \varepsilon_2^2} - \varepsilon_1}{2}}. \quad (4)$$

The optical properties of ultrathin layers were calculated by us in the *periodic slab model*, traditionally used to study low-dimensional structures [30], in which a vacuum layer is added to a periodically repeated supercell containing the slab. In our calculations, the vacuum size separating the slabs from different periodically repeated supercells (see Figure 1, *b*) was large enough (20 Å) to neglect the interaction of images from different supercells and assume that the approach used correctly describes the optical properties of extremely thin two-dimensional systems. Separately, we note that no other model representations were introduced in this work when calculating the optical properties of 2D structures.

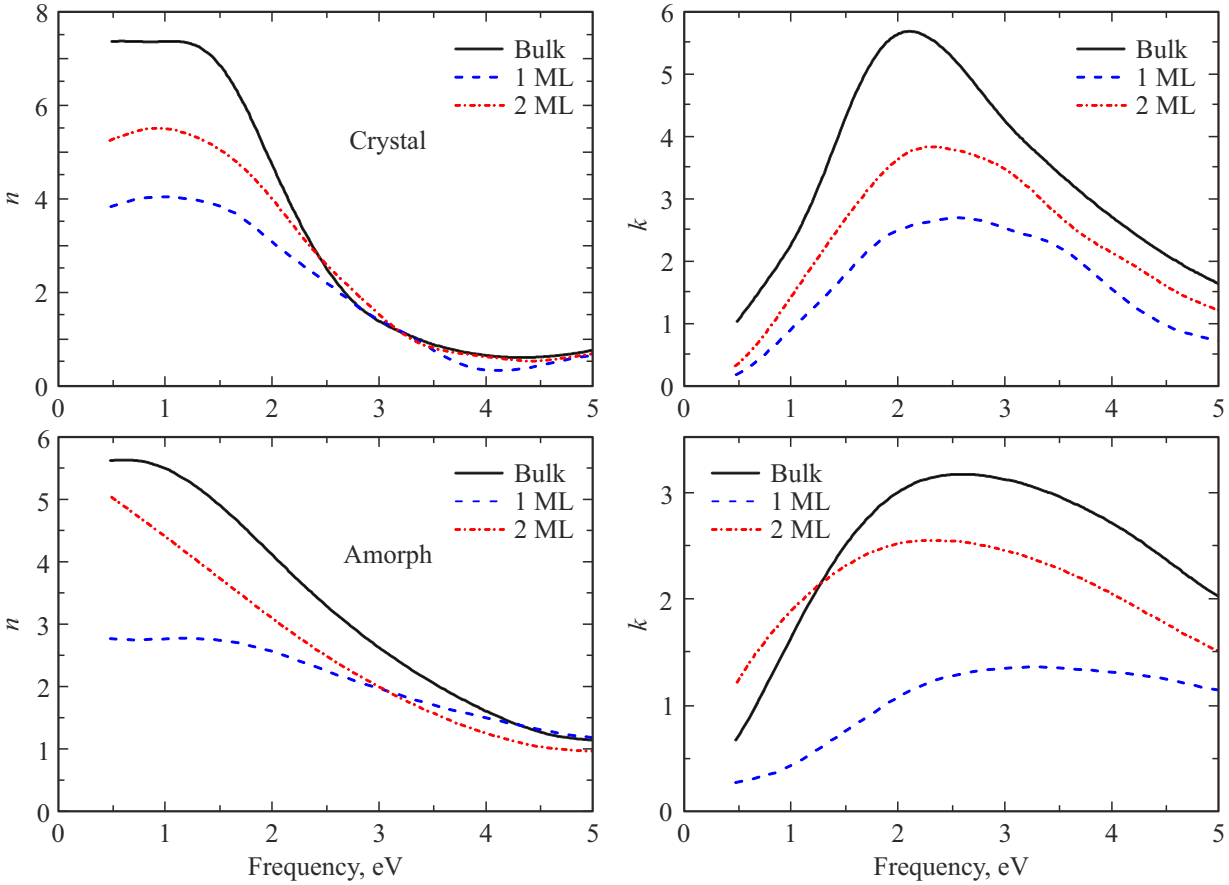

Figure 5. Optical constants for ultrathin layers and bulk materials in crystalline and amorphous phases.

3. Results and discussion

Figure 4 shows the correlation functions for the central antimony and tellurium atoms in the amorphous phase for ultrathin layers and bulk material. Let's first consider the general patterns. First, it's interesting to note that for the amorphous phase strong correlations of Te-Te are traced up to 3–4 of the coordination spheres, while Sb-Sb correlations higher than the second coordination sphere are absent. This result suggests that the tellurium sublattice is the structure-forming element. Apparently, the crystallization process can be considered as the initial ordering of the tellurium sublattice followed by the alignment of the antimony sublattice.

It is interesting to note that the concentration of Te-Te and Sb-Sb bonds (peak intensity at distances ~ 3 Å) in the amorphous structure is significantly less than that of Sb-Te bonds, which suggests that the amorphous phase remains to a large extent chemically ordered. It is also seen that the intensity of Te-Te peak in the bulk material is somewhat lower than the intensity of the Sb-Sb peak, despite the higher content of tellurium atoms, which indicates the energy disadvantage of such bonds. Note also that the peak intensity ratio ($I_{\text{Te-Te}}/I_{\text{Sb-Sb}}$) increases during the transition from layer 1QL to layer 2QL, which is probably due to the fact that during amorphization in the latter, atomic layers formed by tellurium atoms on different sides of the van der Waals gap begin to chemically interact with each other.

Let's consider the impact of thickness on the optical constants of Sb_2Te_3 layers. At the same time, we note that the optical constants were calculated neglecting the spin-orbit interaction, since taking into account the spin-orbit in the calculations of optical properties is not implemented in CASTEP code we use, despite the fact that the spin-orbit impact on the optical properties of the material is of some interest.

Let's first consider the crystalline phase (Figure 5). The refractive index n rises monotonously with increasing layer thickness in the energy range < 2 eV, while in the energy range > 2.5 eV, the dependence of the refractive index on the thickness practically disappears. As for the extinction coefficient k, its value increases throughout the energy range, while the peak value shifts slightly to the low energy range (from 2.5 eV for 1QL to 2.1 eV for bulk material). Such a change in optical constants correlates well with a decrease in the band gap of Sb_2Te_3 layer as the thickness of the layer becomes larger.

In the amorphous phase, the trends in the change of optical constants from the layer thickness are generally preserved, but some features are observed for 2QL layer.

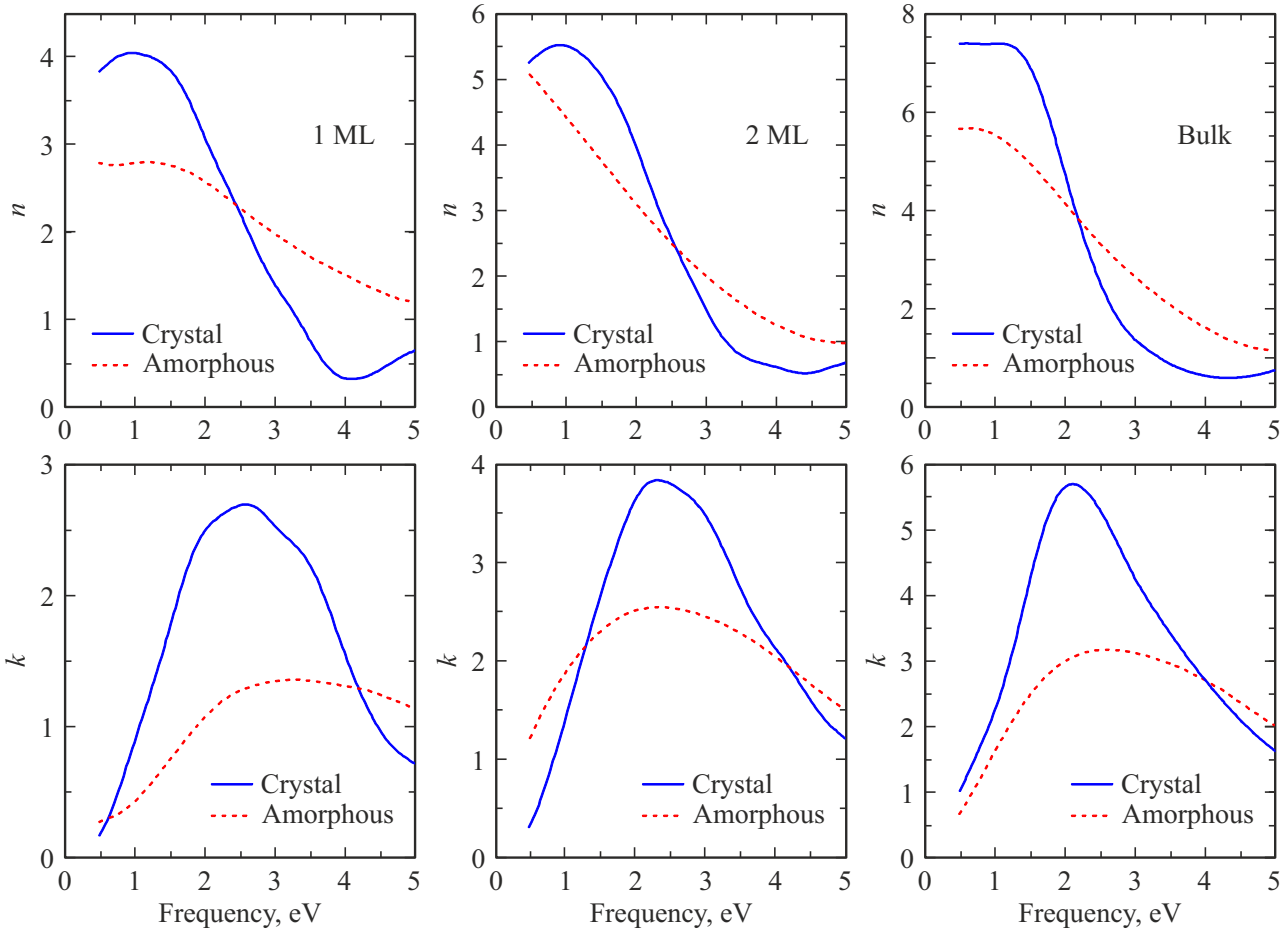

Figure 6. Comparison of optical constants for crystalline and amorphous phases of layers 1QL, 2QL and bulk material.

In particular, while the refractive index goes down or becomes saturated for layer 1QL and bulk material in the low-energy region, for layer 2QL it continues to rise with decreasing energy. Note that this difference has no practical significance, since the instrument structures use light with higher photon energies.

Figure 6 illustrates the optical constants for the crystalline and amorphous phases of layers 1QL, 2QL and bulk material, compared. First and foremost, it should be underscored here that the contrast in optical properties remains up to the minimal possible thickness of Sb_2Te_3 (1QL) layer. Qualitatively, the dependences for layers of different thicknesses are similar, but the focus is made on the fact that in the area of ~ 1 eV — and it is in this area that optical communication lines operate — the greatest optical contrast is observed for 1QL, which indicates the prospects of using ultrathin layers of phase-change Sb_2Te_3 in tunable photonics devices and photonic neuromorphic networks [8]. The practical difficulty in implementing such systems may be the need for precision thickness control, since, as can be seen from Figure 6, the 2QL layer does not have the necessary contrast properties.

4. Conclusion

This study delves into dependence of the optical constants of Sb_2Te_3 as an phase-change material on its layer thickness. A monotonous increase in the refractive index and extinction coefficient of the crystalline phase was observed with an increase in the material thickness, which was in good agreement with a band gap decline. It is demonstrated that during the amorphization-crystallization process, the change in the contrast of optical constants generally does not depend on the layer thickness and persists up to layers with a thickness of one monolayer, which indicates the prospects of using extremely thin phase-change layers in tunable photonics devices.

It was also found that the tellurium sublattice in the amorphous phase is significantly more ordered than the antimony sublattice, which proves the structure-forming role of tellurium.

Acknowledgments

AVK is grateful to Herzen University for the support of this study within the internal grant No. 57-VG; VGK performed the work within the state assignment of the Ministry

of Education and Science of the Russian Federation (subject FFUG-2024-0042). Some calculations were carried out using a supercomputer of Ioffe Physical-Technical Institute.

Conflict of interest

The authors declare that they have no conflict of interest.

References

[1] S. Raoux, M. Wuttig (eds). *Phase-change materials: Science and Applications* (Springer New York, N.Y., 2009).
[2] A.V. Kolobov, J. Tominaga. *Chalcogenides: metastability and phase-change phenomena* (Springer Cham, 2012).
[3] A. Redaelli (ed). *Phase Change Memory: Device Physics, Reliability and Applications* (Springer Verlag, Berlin–Heidelberg, 2018) p. 330.
[4] T. Ohta, S.R. Ovshinsky. *Photo-induced metastability in amorphous semiconductors*, ed. by A.V. Kolobov (WILEY-VCH GmbH & Co. KGaA, Weinheim, 2003) p. 310.
[5] https://www.galex.ru/news/it/3256/
[6] https://club.dns-shop.ru/blog/t-101-ssd-nakopiteli-2-5/36065-chto-takoe-intel-optane-v-ssd-nakopitelyah-i-dlya-chego-eto-nujno/?utm_referrer=https://www.google.com/
[7] M. Xu, X. Mai, J. Lin, W. Zhang, Y. Li, Y. He, H. Tong, X. Hou, P. Zhou, X. Miao. Adv. Funct. Mater., **30**, 2003419 (2020). DOI: 10.1002/adfm.202003419
[8] X. Chen, Y. Xue, Y. Sun, J. Shen, S. Song, M. Zhu, Z. Song, Z. Cheng, P. Zhou. Adv. Mater., **35**, 2203909 (2023). DOI: 10.1002/adma.202203909
[9] V. Bhatnagar, A. Kumar. Energy Storage, **7**, e70272 (2025). DOI: 10.1002/est2.70272
[10] N. Yamada. MRS Bulletin, **21**, 48 (1996). DOI: 10.1557/S0883769400036368
[11] N. Yamada. Rev. Laser Eng., **28**, 585 (2000). DOI: 10.2184/lsj.28.585
[12] A.V. Kolobov, P. Fons, J. Tominaga. Phys. Rev. B, **94**, 094114 (2016). DOI: 10.1103/PhysRevB.94.094114
[13] H.K. He, Y.B. Jiang, J. Yu, Z.Y. Yang, C.F. Li, T.Z. Wang, D.Q. Dong, F.W. Zhuge, M. Xu, Z.Y. Hu, R. Yang. Mater. Horizons, **9**, 1036 (2022). DOI: 10.1039/D1MH01772A
[14] M.Y. Zhang, Z.X. Wang, Y.N. Li, L.Y. Shi, D. Wu, T. Lin, S.J. Zhang, Y.Q. Liu, Q.M. Liu, J. Wang, T. Dong. Phys. Rev. X, **9**, 021036 (2019). DOI: 10.1103/PhysRevX.9.021036
[15] X.-P. Wang, X.-B. Li, N.-K. Chen, B. Chen, F. Rao, S. Zhang. Adv. Sci., **8**, 2004185 (2021). DOI: 10.1002/advs.202004185
[16] K. Ding, B. Chen, F. Rao. Mater. Sci. Semicond. Process., **134**, 105999 (2021). DOI: 10.1016/j.mssp.2021.105999
[17] H. Zhang, C.X. Liu, X.L. Qi, X. Dai, Z. Fang, S.C. Zhang. Nature Physics, **5**, 438 (2009). DOI: 10.1038/nphys1270
[18] K.F. Mak, C. Lee, J. Hone, J. Shan, T.F. Heinz. Phys. Rev. Lett., **105**, 136805 (2010). DOI: 10.1103/PhysRevLett.105.136805
[19] D. Dragoni, J. Behler, M. Bernasconi. Nanoscale, **13**, 16146 (2021). DOI: 10.1039/D1NR03432D
[20] J.P. Perdew, K. Burke, M. Ernzerhof. Phys. Rev. Lett., **77**, 3865 (1996). DOI: 10.1103/PhysRevLett.77.3865
[21] M.D. Segall, P.J.D. Lindan, M.J. Probert, C.J. Pickard, P.J. Hasnip, S.J. Clark, M.C. Payne. J. Phys. Condens. Matter, **14**, 2717 (2002). DOI: 10.1088/0953-8984/14/11/301
[22] S.J. Clark, M.D. Segall, C.J. Pickard, P.J. Hasnip, M.I.J. Probert, K. Refson, M.C. Payne, Z. Krist. Cryst. Mater., **220**, 567 (2005). DOI: 10.1524/zkri.220.5.567.65075
[23] S. Grimme. J. Comput. Chem., **27**, 1787 (2006). DOI: 10.1002/jcc.20495
[24] D. Vanderbilt. Phys. Rev. B, **41**, 7892 (1990). DOI: 10.1103/PhysRevB.41.7892
[25] F.C. Mocanu, K. Konstantinou, J. Mavračić, S.R. Elliott. Phys. Status Solidi RRL, **15**, 2000485 (2021). DOI: 10.1002/pssr.202000485
[26] V.G. Kuznetsov, A.A. Gavrikov, M. Krbal, V.A. Trepakov, A.V. Kolobov. Nanomaterials, **13**, 896 (2023). DOI: 10.3390/nano13050896
[27] Yu. Peter, M. Kardona. *Osnovy fiziki poluprovodnikov* (M., Fizmatlit, 2002) (in Russian).
[28] H.J. Monkhorst, J.D. Pack. Phys. Rev. B, **13** (12), 5188 (1976). DOI: 10.1103/PhysRevB.13.5188
[29] A.I. Ansel'm. *Vvedenie v teoriyu poluprovodnikov* (M., Nauka, 1978) (in Russian).
[30] D.S. Sholl, J.A. Steckel. *Density Functional Theory: a practical introduction* (John Wiley & Sons, N.J.).

Translated by T.Zorina